Journal of Power Sources 253 (2014) 230–238

Contents lists available at ScienceDirect

Journal of Power Sources

journal homepage: www.elsevier.com/locate/jpowsour

Star-shaped carbazole derivative based efficient solid-state dye sensitized solar cell

Asta Michaleviciute [a], Martial Degbia [b], Ausra Tomkeviciene [a], Bruno Schmaltz [b], Egle Gurskyte [a], Juozas Vidas Grazulevicius [a,*], Johan Bouclé [c], François Tran-Van [b,*]

[a] Department of Organic Technology, Kaunas University of Technology, Radvilenu pl. 19, LT-50254 Kaunas, Lithuania
[b] Université F. Rabelais, Laboratoire de Physico-Chimie des Matériaux et des Electrolytes pour l'Energie (PCM2E), EA 6299, Parc de Grandmont, 37200 Tours, France
[c] Institut XLIM UMR 7252, Université de Limoges/CNRS, 123 av. A. Thomas, 87060 Limoges Cedex, France

HIGHLIGHTS

- Star shape carbazole molecular glasses were synthesized and characterized.
- Optical and energy level of the molecule are well adapted for D102 based DSSC.
- ssDSSC using the carbazole derivative shows higher J_{sc} than the spiro-OMeTAD.
- Power conversion efficiency of 2.23% was obtained without optimization.

GRAPHICAL ABSTRACT

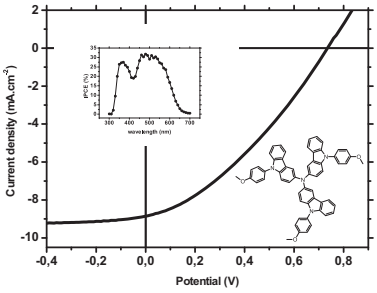

ARTICLE INFO

Article history:
Received 26 July 2013
Received in revised form
26 November 2013
Accepted 9 December 2013
Available online 18 December 2013

Keywords:
Carbazole
Molecular glass
Star-shaped structure
Solid-state dye sensitized solar cells

ABSTRACT

Two new star-shaped carbazole molecules, including tri(9-(methoxyphenyl)carbazol-3-yl)amine named TMPCA having molecular glasses properties and hole transport properties were synthesized. Their thermal, optical, photophysical and electrochemical properties were studied. The carbazole based molecules exhibit high thermal stability with 5% weight loss temperatures over 480 °C with higher glass temperature transitions 164–175 °C than the classical spiro-OMeTAD reference molecule. Their optical band gaps (2.76 eV) are low enough not to hinder neither the absorption of the indoline sensitizer (D102) nor its photoexcitation and charge transfer. Solid state ionization potential (IPs) of TMPCA is well adapted to that of D102 and ensure a driving force ΔrG >0.2 eV for an efficient transfer and regeneration of the photo-oxidized dye. Solid-state dye sensitized solar cells ITO/TiO_2/D102/T4MPCA/Au showed a power conversion efficiency of 2.23% with J_{sc} of 8.85 mA cm^{-2} under standard AM 1.5 simulated solar irradiation.

1. Introduction

Due to the lack of fossil fuels and the race towards low cost and high energy conversion efficiency, organic or hybrid solar cells have drawn much attention [1–4]. Among them, Dye Sensitized Solar Cells (DSSC) have attracted increasing interest in the last decade and is now appearing as a serious potential alternative to silicon-based photovoltaic devices. DSSCs with high conversion efficiencies over 11–12% using dyes based on Ruthenium complex [5,6] or zinc porphyrine [7] have been prepared. Usually, such a high performance is obtained in DSSC with a liquid electrolyte containing an iodide/triiodide (I^-/I_3^-) or

* Corresponding authors.
E-mail addresses: Juozas.Grazulevicius@ktu.lt (J.V. Grazulevicius), francois.tran@univ-tours.fr (F. Tran-Van).

0378-7753/$ – see front matter © 2013 Elsevier B.V. All rights reserved.
http://dx.doi.org/10.1016/j.jpowsour.2013.12.039

cobalt (II/III) based redox system prepared in solution with acetonitrile.

However, such cells suffer from potential leakage problems associated with the corrosive and volatile nature of the liquid electrolyte and, thus, may not be practical for large-scale applications [8]. Recent efforts therefore have been devoted on substituting the liquid electrolyte with solid or quasi-solid electrolytes. In solid-state DSSC (ssDSSC), a solid hole transporting material (HTM) is used such as the well-known 2,2′,7,7′-tetrakis(*N*,*N*-di-*p*-methoxyphenylamine)-9,9′-spirobifluorene (spiro-OMeTAD). Compared to conjugated polymers [9], amorphous metastable low molecular weight compound named molecular glasses possess the advantage to be easily incorporated inside the mesoporous titanium oxide and to improve pore filling [10,11].

Since few years, spiro-OMeTAD is showing increasing performances organic dyes such as D102 (4.1%) [12], or Y123 (7.2%) [13] dyes. More recently, power conversion efficiency reaching 15% by combining perovskite as sensitizer and spiro-OMeTAD as HTM has been achieved [14]. However, nowadays, the reference spiro-OMeTAD HTM remains still too expensive for large-scale applications. That is why the development of cheaper molecular glasses is a crucial challenge. Although, in the literature, only few alternatives are described and able to compete with it, amorphous small molecules based on carbazole moieties have already been reported [15–17].

In the aim of increasing the range of cheap amorphous low-molar-mass compounds available for the realization of solid-state DSSCs, we have synthesized star-shaped carbazole derivatives. Possessing a nitrogen core, these molecules have a tri-dimensional star-shaped structure. Their thermal, optical, photoelectrical and electrochemical properties have been studied. Preliminary results on FTO/TiO_2/D102/molecular glass/Au solid-state DSSC are also presented and show promising results.

2. Experimental details

2.1. Materials

9-(4-Methoxyphenyl)carbazole [18], *9-(2-methoxyphenyl)carbazole* [19], *3-amino-9-(4-methoxyphenyl)carbazole* (**2a**) [20] were synthesized by the reported procedures. 3-Nitro-9-(2-methoxyphenyl) carbazole (**1b**) was obtained by a slightly modified procedure [21] (Table 1). To a solution of 9-(2-methoxyphenyl)carbazole (2.2 g, 8.1 mmol) in glacial acetic acid (30 ml), nitric acid (0.4 ml, 8.9 mmol) was slowly added. The mixture was refluxed for 4 h. The resulting solution was poured into water. The precipitate was collected by filtration and dried under vacuum. Yield: 1.6 g (62%) of a yellow solid. ^{1}H NMR (300 MHz, $CDCl_3$), δ (ppm): 3.76 (s, 3H, $-OCH_3$), 7.14–7.29 (m, 4H, Ar), 7.38–7.62 (m, 4H, Ar), 8.21–8.24 (m, 1H, Ar), 8.31–8.35 (m, 1H, Ar), 9.11–9.16 (m, 1H, Ar). MS (ACPI+, 20 V), *m*/*z* (%): 319 ([M + H]$^+$, 80).

3-Amino-9-(2-methoxyphenyl)carbazole (**2b**). 3-Nitro-9-(2-meth oxyphenyl)carbazole (1.58 g, 4.9 mmol), $SnCl_2$ (4.7 g, 24.8 mmol), acetic acid (50 ml) and concentrated hydrochloric acid (35%, 5 ml) were placed into a round-bottom flask. The mixture was refluxed under argon for 24 h. The resulting solution was poured into an aqueous sodium hydroxide solution (20%, 250 ml). The mixture was extracted with ethyl acetate. The organic phase was dried over Na_2SO_4, filtrated and concentrated under vacuum. The residue was purified by column chromatography using hexane/ethyl acetate (3/1) as an eluent. Yield: 1.54 g (92%) of **2b**. ^{1}H NMR (300 MHz, $CDCl_3$), δ (ppm): 3.73 (s, 3H, $-OCH_3$), 5.54 (s, 2H, $-NH_2$), 6.86–7.50 (m, 10H, Ar), 8.08 (s, 1H, Ar). MS (ACPI+, 20 V), *m*/*z* (%): 289 ([M + H]$^+$, 80).

3-Iodo-9-(4-methoxyphenyl)carbazole (**3a**) was prepared by Tucker iodination reaction [22]. 9-(4-Methoxyphenyl)carbazole (3.4 g, 12.5 mmol), potassium iodide (2.3 g, 13.7 mmol), potassium iodate (2.9 g, 13.7 mmol) were refluxed in 250 ml of acetic acid for 4 h. The crystallized product (at ambient temperature) was washed several times with methanol and dried under vacuum. Yield: 4.8 g (96%) of **3a**. ^{1}H NMR (300 MHz, $CDCl_3$), δ (ppm): 3.96 (s, 3H, $-OCH_3$), 7.12–7.17 (m, 2H, Ar), 7.29–7.51 (m, 6H, Ar), 7.66–7.69 (m, 1H, Ar), 8.19 (d, 1H, J = 7.71 Hz, Ar), 8.50 (s, 1H, Ar). MS (ACPI+, 20 V), *m*/*z* (%): 400 ([M + H]$^+$, 70).

3-Iodo-9-(2-methoxyphenyl)carbazole (**3b**) was prepared according the same procedure as **3a**.Yield : 94%. ^{1}H NMR (300 MHz, $CDCl_3$), δ (ppm): 3.74 (s, 3H, $-OCH_3$), 7.16–7.23 (m, 4H, Ar), 7.27–7.34 (m, 2H, Ar), 7.39–7.57 (m, 4H, Ar), 7.64–7.68 (m, 1H, Ar). MS (ACPI+, 20 V), *m*/*z* (%): 400 ([M + H]$^+$, 80).

Tri(9-(4-methoxyphenyl)carbazol-3-yl)amine (T4MPCA). 3-Amino-9-(4-methoxyphenyl)carbazole (**2a**, 1.7 g, 5.9 mmol), 3-iodo-9-(4-methoxyphenyl)carbazole (**3a**, 4.7 g, 11.8 mmol), potassium carbonate (4.89 g, 35.4 mmol), copper powder (1.49 g, 23.6 mmol) and 18-crown-6 (0.2 g) were refluxed in 25 ml of *o*-dichlorobenzene under nitrogen for 24 h. Then, copper and inorganic salts were filtered off. The solvent was distilled off and the product was purified by column chromatography using hexane/ethyl acetate (20/1) as an eluent and recrystallized from the same eluent mixture. Yield: 0.98 g (20%) of T4MPCA (mp: 264–265 °C). ^{1}H NMR (300 MHz, DMSO-d_6), δ (ppm): 3.87 (s, 9H, $-OCH_3$), 7.12 (t, 3H, J = 7.25 Hz, Ar), 7.18–7.27 (m, 14H, Ar), 7.37 (t, 4H, J = 7.6 Hz, Ar), 7.52–7.55 (d, 6H, J = 6.69 Hz, Ar), 7.95 (s, 3H, Ar), 7.99 (d, 3H, J = 7.8 Hz, Ar). ^{13}C NMR (100 MHz, DMSO-d_6), δ (ppm): 55.5 ($-OCH_3$), 107.9, 109.0, 110.1, 111.0, 114.7, 115.9, 119.1, 119.3, 120.6, 120.8, 122.2, 123.0, 125.8, 140.5, 141.3. Elemental analysis. Calcd. for $C_{57}H_{42}N_4O_3$ (%): C 82.39, H 5.09, N 6.74, O 5.78. Found (%): C 82.53, H 5.29, N 6.83. IR (KBr), (ν/cm^{-1}): 3044, 3000 (C–H Ar); 2951, 2931 (C–H); 1574, 1514, 1477, 1456 (C=C Ar); 1368, 1345, 1319 (C–N). MS (ACPI+, 20 V), *m*/*z* (%): 831 ([M + H]$^+$, 100).

Tri(9-(2-methoxyphenyl)carbazol-3-yl)amine (T2MPCA) was prepared from 3-amino-9-(2-methoxyphenyl)carbazole (**2b**, 1.9 g, 6.6 mmol), 3-iodo-9-(2-methoxyphenyl)carbazole (**3b**, 5.26 g, 13.2 mmol) powdered potassium carbonate (5.46 g, 39.6 mmol), copper powder (1.68 g, 26.4 mmol) and 18-crown-6 (0.2 g) in the same way as T4MPCA. The product was purified by column chromatography using hexane as an eluent and recrystallized from hexane. Yield: 1.1 g (20%) of T2MPCA (mp: 175–176 °C). ^{1}H NMR (300 MHz, DMSO-d_6), δ (ppm): 3.81 (s, 9H, $-OCH_3$), 7.21–7.26 (m, 14H, Ar), 7.37 (t, 4H, J = 7.35 Hz, Ar), 7.28–7.49 (m, 7H, Ar), 7.97–7.99 (m, 8H, Ar). ^{13}C NMR (100 MHz, DMSO-d_6), δ (ppm): 56.2 ($-OCH_3$), 107.8, 109.9, 110.3, 112.3, 113.1, 115.7, 119.6, 119.3, 120.7, 121.5, 122.8, 123.0, 126.0, 139.9, 141.3. Elemental analysis. Calcd. for $C_{57}H_{42}N_4O_3$ (%): C 82.39, H 5.09, N 6.74, O 5.78. Found (%): C 82.52, H 5.21, N 6.82. IR (KBr), (ν/cm^{-1}): 3045 (C–H Ar); 2959, 2931 (C–H); 1596, 1508, 1479, 1461 (C=C Ar); 1366, 1302 (C–N). MS (ACPI+, 20 V), *m*/*z* (%): 831 ([M + H]$^+$, 100).

2.2. Instrumentation

^{1}H NMR and ^{13}C NMR spectra were recorded using Avance III 400 spectrometer [400 MHz (^{1}H), 100 MHz (^{13}C)]. Mass spectra were obtained on a Waters ZQ 2000 spectrometer. Infrared (IR) spectra were recorded using Perkin Elmer Spectrum GX spectrometer. The spectra of solid compounds were performed using KBr pellets. Mass (MS) spectra were obtained on a Waters ZQ 2000 (Waters, Milford, USA).

Differential scanning calorimetry (DSC) measurements were carried out using a Perkin–Elmer DSC-7 series thermal analyzer. Thermogravimetric analysis (TGA) was performed on a Netzsch STA 409. The TGA and DSC curves were recorded under nitrogen atmosphere at a heating rate of 10 °C min^{-1}.

Table 1
Chemical structure of the synthesized carbazole derivatives.

Name	Structure	Name	Structure
1a	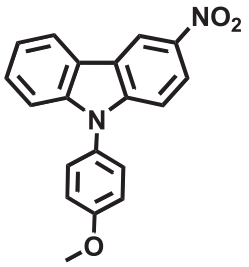	**3a**	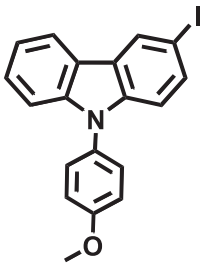
1b	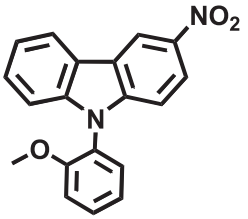	**3b**	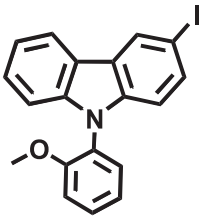
2a	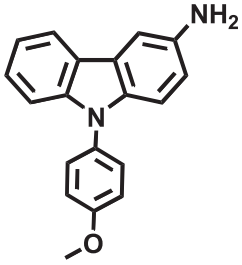	T4MPCA	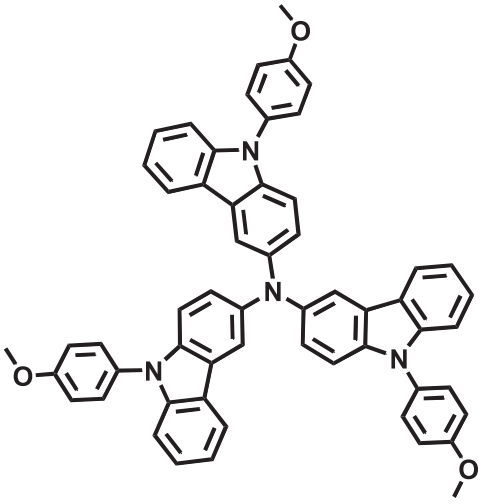
2b	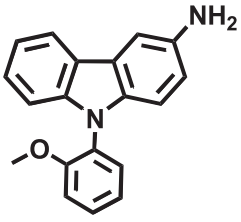	T2MPCA	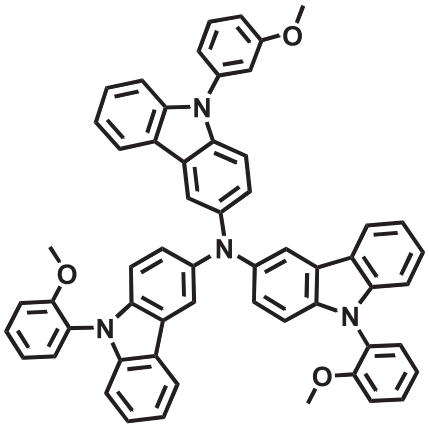

Ultraviolet–visible (UV–vis) absorption spectra were recorded with Hitachi U-3000 and Spectronic Unicam Genesys 8 spectrometers. Fluorescence (FL) spectra were recorded with a Hitachi MPF-4 spectrometer (resolution 2 nm). Dilute solutions (10^{-5} mol L^{-1}) of the materials in tetrahydrofuran (THF) were used for the UV–vis absorption and FL measurements.

The cyclic voltammetry (CV) measurements were carried out by a three-electrode assembly cell from Bio-Logic SAS and a

micro-AUTOLAB Type III potentiostat-galvanostat. The measurements were carried out with a glassy carbon electrode in dichloromethane solutions containing 0.1 M tetrabutylammonium perchlorate (TBAP) as electrolyte, $Ag/AgNO_3$ 0.01 M as the reference electrode, and a Pt wire counter electrode. All the experiments were calibrated with the standard ferrocene/ferrocenium redox system as internal reference.

The ionization energies (E_I) of thin layers of the materials were measured by electron photoemission method in air as described earlier [23,24]. The samples for the ionization energy measurements were prepared as reported previously [23]. The active materials were dissolved in THF and were coated on Al plates precoated with ca. 0.5 μm thick adhesive layer of methyl methacrylate and methacrylic acid copolymer (MKM). The function of this layer was not only to improve adhesion, but also to eliminate the electron photoemission from Al layer. In addition, the MKM layer is conductive enough to avoid charge accumulation during the measurements. The thickness of the layers was 0.5–1 μm.

2.3. Preparation of the devices

F-doped tin oxide glass substrates (FTO, Solaronix TCO2215, 15 Ohm square^{-1}) were subsequently washed in an ultrasonic bath for 10 min in acetone, isopropanol and water. After a final UV-ozone cleaning step (10 min), a compact TiO_2 layer (~200 nm) was deposited by chemical spray-pyrolysis at 450 °C [25] from a solution of titanium tetra-isopropoxide and acetylacetone in ethanol (Sigma–Aldrich) and then annealed at 450 °C for 20 min in air. A mesoporous layer of TiO_2 was spin-coated on the compact layer from a dilute commercial TiO_2 paste (DSL 18NRT, Dyesol), followed by a ramped sintering step in air up to 500 °C over 45 min. The obtained porous electrode (2 μm thick) were then immersed in a 0.02 M aqueous $TiCl_4$ solution for 2 h at room temperature [26,27] before rinsing and sintered at 500 °C for 45 min. The sensitization of the nanocrystalline electrode was realized by soaking the film in a 0.6 mM solution of indoline D102 dye (Mitsubishi Paper Mills, Japan) in a mixture of acetonitrile:*tert*-butanol (1:1 vol%) (Sigma–Aldrich) overnight at 80 °C. After rinsing with acetonitrile, the dye-sensitized electrode was infiltrated with the organic hole conductor by spin coating from a solution of either spiro-OMeTAD or T4MPCA in chlorobenzene (Sigma–Aldrich) at 200 mg ml^{-1}. $Li(CF_3SO_2)_2N$ and *tert*-butylpyridine additives were used in all cases, following conventional procedures reported in the literature [28]. Before spin-coating, the solution of hole-transporting material was heated at 100 °C to ensure a complete solubilization. The solution was then dispensed on the dye-sensitized substrates for 40 s before the rotation.

Gold top electrodes were finally evaporated under vacuum using shadow masks that define two active areas per substrates (0.18 cm^2 each).

The current density–voltage (J–V) characteristics were recorded in air using a Keithley 2400 source-measure unit, in the dark and under simulated solar emission (ORIEL, 1600W, AM1.5G). The spectral mismatch between the emission of the solar simulator and the global AM1.5G solar spectrum (ASTM G173-03) was corrected using a mismatch factor [29] and the solar simulator irradiance was adjusted accordingly using a certified silicon reference cell in order to achieve an equivalent irradiance of one sun (100 mW cm^{-2}) on the test cells.

3. Results and discussion

3.1. Synthesis

The synthetic route to the star-shaped tri(9-(methoxyphenyl) carbazol-3-yl)amine T2MPCA and T4MPCA is shown on Fig. 1. The target molecules were synthesized by a Ullmann coupling reaction from the two carbazole derivative units **2a**,**b** and **3a**,**b**. The preparation of both units was started from the functionalization of 9-methoxyphenyl-carbazole in C-3 position by a nitro- (**1a**,**b**) and an iodo group (**3a**,**b**) respectively with nitric and mixture KI/KIO_3. The Tucker iodination reaction gave 3-iodo-9(methoxyphenyl) carbazole (**3a**,**b**) with the yield over 90%. The preparation of **2a**,**b** was a two-step synthesis involving nitration then reduction reactions, leading to the introduction of the amino-group in C-3 position of the carbazole moiety, with an over yield around 60%. Finally, the star shape target molecules T2MPCA and T4MPCA were synthesized by reacting one equivalent of 3-amino-9-

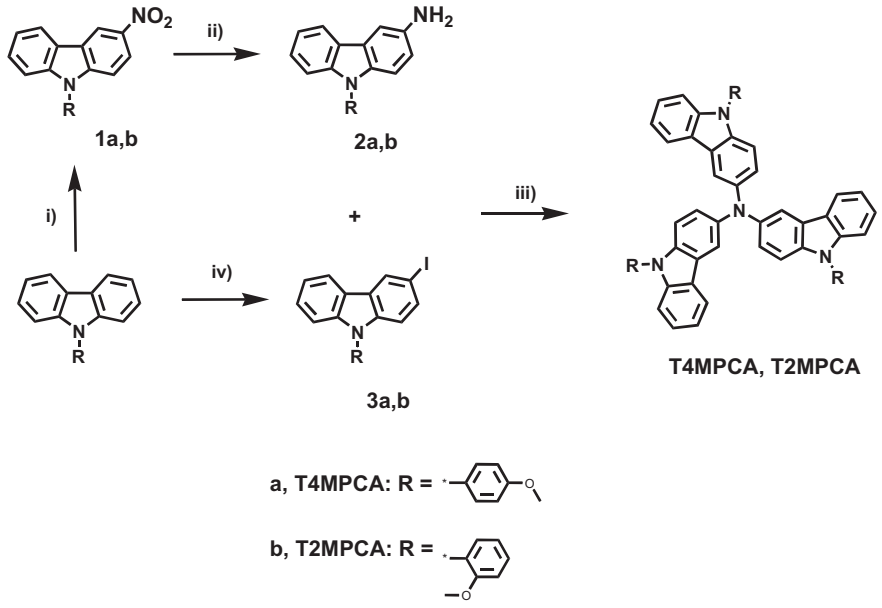

Fig. 1. Synthesis of T4MPCA and T2MPCA. Reagents and conditions: (i) acetic acid, HNO_3, 4 h, (ii) $SnCl_2$, acetic acid, HCl, 24 h, (iii) K_2CO_3, Cu, 18-crown-6, o-dichlorobenzene, 180 °C, 24 h, (iv) KI, KIO_3, acetic acid, 4 h.

(methoxyphenyl)carbazole (**2a**,**b**) with two equivalents of 3-iodo-9-(methoxyphenyl)carbazole (**3a**,**b**) in *o*-dichlorobenzene using Ullmann conditions (20% yield). ^{1}H and ^{13}C NMR, IR, mass spectrometry and elemental analysis confirmed that the target molecules were obtained.

T2MPCA and T4MPCA differ only by the position of –OMe groups in the methoxyphenyl subunit. The difference has an effect on the solubility of the final product. T4MPCA have better solubility in common organic solvents such as THF, acetone, chloroform.

3.2. Thermal properties

The behavior under heating of T4MPCA and T2MPCA was studied by DSC and TGA. Both molecules show high thermal stability as demonstrated by their high values of T_{ID} (5% weight loss temperature). T4MPCA and T2MPCA showed respectively a T_{ID} of 490 °C and 480 °C which are higher than those of carbazole derivatives mono and difunctionalized with di-methoxy phenyl groups [16]. T4MPCA and T2MPCA were obtained as crystalline materials; however they can be transformed in to a quasi-stable solid amorphous state. The DSC thermograms of T4MPCA are shown in Fig. 2. The sample of T4MPCA revealed melting transition at 262 °C during the first DSC heating scan. No crystallization exotherm and melting endotherm were observed in the following cooling and heating scans. Only one endothermic signal assigned to a glass transition was observed at 164 °C which is characteristic of a molecular glass behavior. No changes were observed after successive melting/cooling cycles indicating that the amorphous state is meta-stable. It can be noticed that the stable amorphous state of the hole transporting materials is crucial to ensure a suitable interface between the semi-conductor organic layer and the sensitized titanium oxide. The values of the glass transition temperature are quite high in comparison with those of the standard hole transporting material used in the solid-state DSSC i.e. spiro-OMeTAD (120 °C) [30]. These values are also considerably higher than those observed for the promising difunctionalized carbazoles recently published by our group as hole-transporting materials for high efficiency solid state DSSC [15]. These higher T_g are expected to improve the stability of the amorphous state of the HTM and the stability of the ssDSSC without structural reorganization such as crystallization of the organic semiconducting layer even at high temperature.

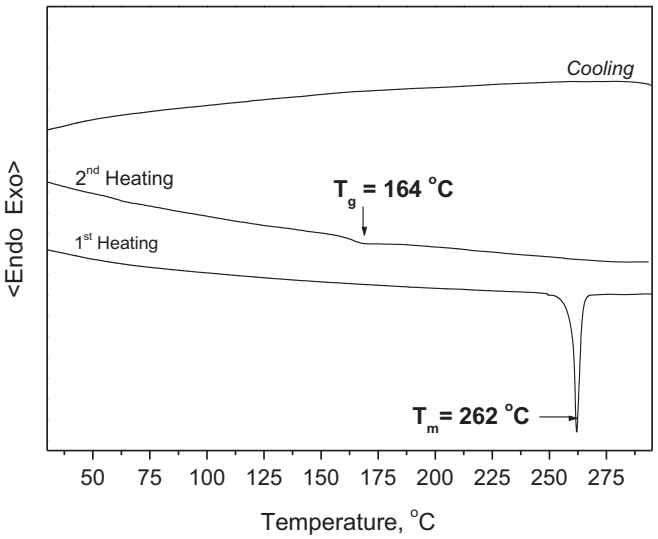

Fig. 2. DSC curves of T4MPCA (heating rate 10 °C min^{-1}, N_2 atmosphere).

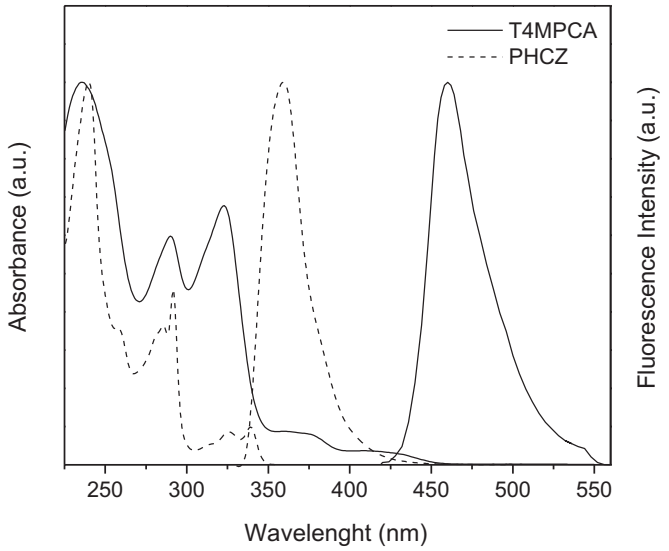

Fig. 3. Absorption and normalized fluorescence (λ_{ex} = 320 nm) spectra of the dilute (10^{-5} M) THF solutions of T4MPCA and PHCZ.

3.3. Optical properties

UV–vis absorption and fluorescence (FL) spectra of dilute THF solutions of T4MPCA are shown in Fig. 3. The wavelengths of the different absorption bands are listed in Table 1. T4MPCA exhibits the main absorption peak at 322 nm associated with the π–π* transition and two other bands weak in intensity at 375 nm and 420 nm. For the comparison, the UV–vis spectrum of 9-phenylcarbazole (PHCZ) is given in Fig. 3. T4MPCA demonstrates a red shift of the absorption with respect of PHCZ. This increase of conjugation along the molecule shows that an electronic delocalization through the central nitrogen atom of T4MPCA occurs. The FL emission spectra of the synthesized stars also show red shifts by ca. 100 nm compared to the PHCZ spectrum. Although the electronic delocalization is increased through the T4MPCA, the material does not absorb in the visible range. It means that, associated with a specific dye such as the classical (5-(1,2,3,3a,4,8b-hexahydro-4-[4-(2,2-diphenylvinyl) phenyl]-cyclopeanta[*b*]indole-7-ylmethylene)-4-oxo-2-thioxo-thiazolidin-3-yl)acetic acid named D102 (λ_{max} = 501 nm), the hole-transporting molecular glass cannot hinder neither the absorption of the dye nor its photoexcitation and charge transfer. The optical band gaps (E_g^{op}), evaluated from the absorption edges of the spectra of diluted solution are 2.76 eV for both compounds, which is slightly lower than that of the spiro-OMeTAD (2.98 eV) [17]. Moreover, as expected, the ortho position of the methoxy group of the star-shaped structure (T2MPCA) does modify neither the absorbance nor the fluorescence spectrum compared to those of T4MPCA (see Table 2).

3.4. Electrochemical and photoelectrical properties

The cyclic voltammograms of the dilute solutions of T4MPCA and T2MPCA in dichloromethane/0.1 M tetrabutylammonium

Table 2
Thermal, optical and energetic characteristics of T4MPCA and T2MPCA.

Compound	T_g (°C)	T_m (°C)	T_{ID} (°C)	UV, λ_{max} (nm)	FL, λ_{max} (nm)	E_g^{op} (eV)
T4MPCA	164	262	490	322, 375, 420	460	2.76
T2MPCA	175	308	480	322, 374, 420	460	2.76
PHCz				293, 327, 340	359	3.57

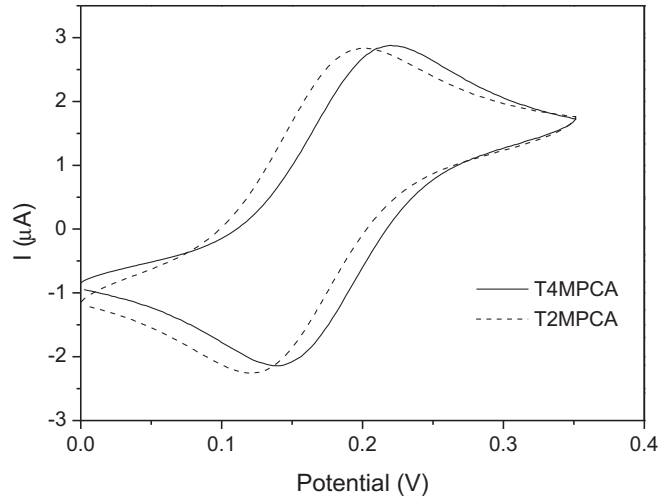

Fig. 4. Cyclic voltammograms of T4MPCA and T2MPCA (scan rate = 20 mV s^{-1}) in argon-purged dichloromethane solution (10^{-3} M tetrabutylammonium perchlorate). Ref: Fc/Fc^{+}.

perchlorate showed one reversible redox couple (Fig. 4). T4MPCA showed an oxidation potential peak E_{pa} of 0.22 V (vs $Fc:Fc^{+}$) and a $E_{1/2}$ [defined as $(E_{pa} + E_{pc})/2$] of 0.18 V. Meanwhile T2MPCA showed an oxidation potential peak E_{pa} of 0.20 V (vs $Fc:Fc^{+}$) and $E_{1/2}$ of 0.16 V. In both measurements, the value of the ΔE_p [defined as $(E_{pa} - E_{pc})$] was around 0.08 V which indicate a quasi-reversible mono-electronic process.

T4MPCA, T2MPCA possess open reactive C-6 position but exhibit stable redox system since the formation of radical cations during the oxidation did not lead to the creation of a new signal of carbazole dimer as classically observed for monosubstituted carbazole [31]. Moreover, repetitive cycling did not give the increasing currents characteristic of polymerization/crosslinking as it would be the case for a coupling of cation radical of carbazole moieties.

The radical cation formed during the anodic process could be due to the oxidation of the nitrogen core of the star-shaped structure. By comparison the oxidation process of triphenylamine molecule shows the first reversible redox system at $E_{1/2}$ 0.33 V (with $\Delta E_p = 0.14$ V). The carbazole moieties would more effectively stabilize the oxidized species of the molecule by comparison to phenyl groups.

In order to determine the energetic conditions for energy and electron transfer in the device, the solid state ionization potential (IPs) and solid state Electron Affinity (EAs) values were calculated from electrochemistry and optical measurements.

The IPs is estimated from the $E_{1/2}$ of the redox system of T4MPCA and T2MPCA at 4.98 eV and 4.96 eV respectively (based on the relation $IPs = eE_{1/2}^{+/\circ} + 4.8$ eV where e is the electronic charge and where the potential is relative to ferrocenium/ferrocene [32–34]. The EAs of T4MPCA and T2MPCA were determined from the relation $EAs = IPs - E_g^{opt}$ where E_g^{opt} is an estimate of the energy of the first singlet excited state, 0–0 transition). The values are respectively 2.22 eV and 2.20 eV. All the electrochemical and energy levels values are resumed in Table 3.

The Ionization Energy of T4MPCA and T2MPCA were also measured by the electron photoemission (E_I) as described in the literature [17] and the results are presented in Fig. 5 and Table 2. The organic materials investigated were stable enough to perform the measurements in air. The E_I values of both compounds were found to be comparable, i.e. 4.96 eV and 4.92 eV respectively for T4MPCA and T2MPCA and closed to the IPs values obtained by the

Table 3
Electrochemical characteristics and IPs and EAs of T4MPCA and T2MPCA.

Compound	E_{pc} (V)	E_{pa} (V)	$E_{1/2}$ (V)	IP_s^e (eV)	EA_s (eV)	E_I[a] (eV)
T4MPCA	0.14	0.22	0.18	−4.98	−2.22	4.96
T2MPCA	0.12	0.20	0.16	−4.96	−2.20	4.91

[a] Ionization energy was measured by the photoemission in air method from films.

electrochemistry way. It is obvious that the values of E_I of the star-shaped carbazole-based derivatives are lower as compared with those of linear carbazole trimers, i.e. 3,6- or 2,7-(9-carbazolyl) disubstituted derivatives of carbazole [35] and with those of the materials containing electronically isolated carbazolyl groups [36]. It would confirm that the central nitrogen atom participate to the electronic delocalization of the carbazole as discussed in the electrochemistry part.

3.5. Photovoltaic properties of solid-state DSSCs and discussion

The photovoltaic properties of solid state DSSC devices containing T4MPCA and T2MPCA as HTMs were estimated under simulated AM 1.5 irradiation condition (100 mW cm^{-2}) by using two electrodes of SnO_2:F (4.7 eV) and Au (5.1–5.4 eV). The commercial indoline D102 dye was used as organic sensitizer, as it makes a relevant reference to assess the new HTM proposed within this work.

As already described in Refs. [37–39], the use of additives with the HTM is generally necessary to improve the photovoltaic performance of the device. First, lithium bistrifluoromethanesulfonamide (LiTFSI) is known to increase the performance of the solar cells in terms of photocurrent as well as open circuit voltage [37]. Then, *tert*-butylpyridine is added to allow solubilization of the lithium salt and also to increase the open circuit voltage through various mechanisms described in the literature [38,39].

The photocurrent–voltage (J–V) characteristics of the devices are shown in Fig. 6a. As reference, a solid-state DSSC device has been built using spiro-OMeTAD. The photovoltaic parameters of the devices, such as open-circuit photovoltage (V_{oc}), short-circuit photocurrent density (J_{sc}), fill factor (FF), and solar-to-electrical energy conversion efficiency (η) are summarized in Table 3.

The results obtained with the device containing T4MPCA as HTM show a high J_{sc} value of 8.85 mA cm^{-2} which is slightly higher that the reference cell based on spiro-OMeTAD (8.15 mA cm^{-2})

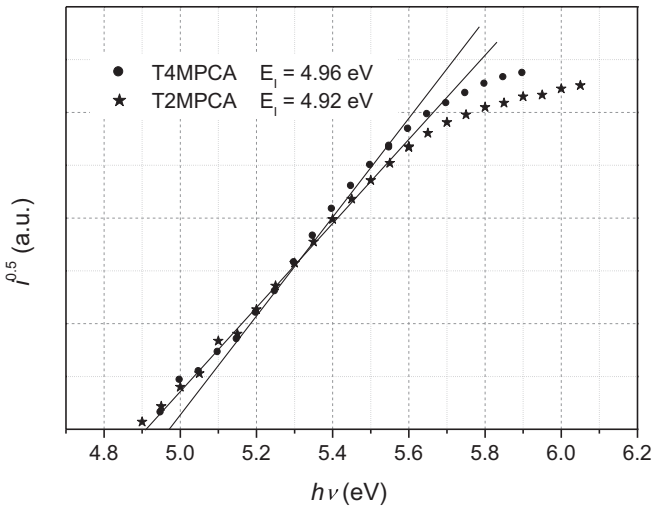

Fig. 5. Electron photoemission spectra of the layers of T4MPCA and T2MPCA.

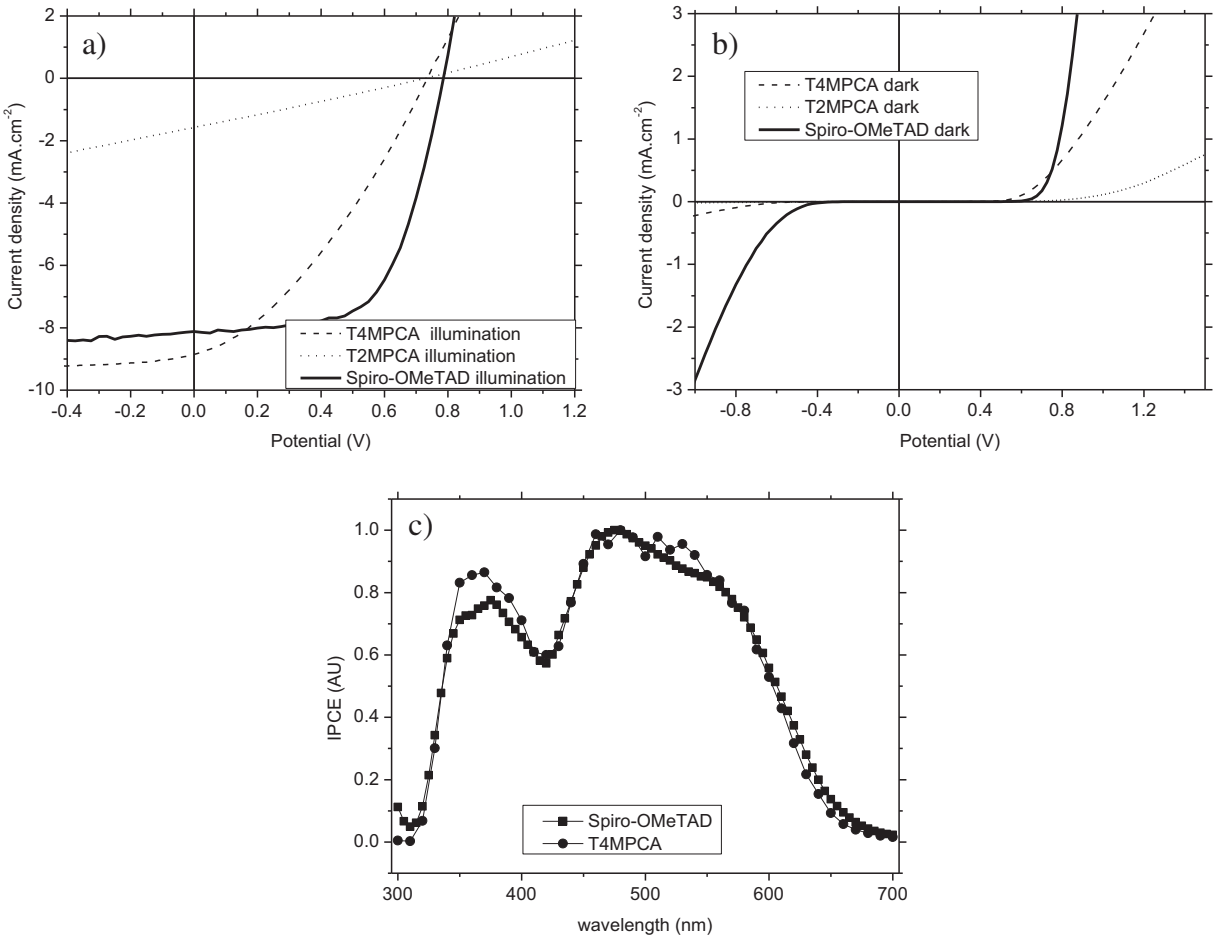

Fig. 6. *J–V* curves of T2MPCA (dot), T4MPCA (dash) and spiro-OMeTAD (solid) a) under illumination of simulated solar light (AM 1.5, 100 mW cm^{-2}); b) in the dark; c) incident-photon-to-current conversion efficiency (IPCE) of devices with spiro-OMeTAD (diamond) and T4MPCA (square).

under the same preparation conditions (Fig. 6a). This result indicates that the regeneration of the photo-oxidized T4MPCA dye and the charge transport to the electrode are efficient. Indeed, IPs of D102: 5.2 eV (evaluated from electrochemistry by CV in the same experimental conditions) and in agreement with the literature [40] is quite well adapted to that of T4MPCA (4.98 eV) for an efficient transfer and regeneration of the photo-oxidized dye [41]. According to our recent results of solid state DSSC using 3,6-di(4,4′-dimethoxydiphenylaminyl)-9-phenylcarbazole as hole transporting layer with similar IPs (4.95 eV), the driving force (defined as $IP_{s(HTM)} - IP_{s(Dye)}$) >0.2 eV is sufficient to ensure high power conversion efficiency [15].

From the *J–V* comparative measurements obtained in the dark (Fig. 6b), the turn on-voltage of the cell containing T4MPCA (around 0.4 V) is lower than that containing piro-OMeTAD (around 0.6 V). The device containing T2MPCA shows the highest turn-on voltage (around 0.7 V). This difference seems to indicate that T4MPCA is slightly less resistive than spiro-OMeTAD and T2MPCA. The T2MPCA seems to be the most resistive HTM among the three molecules due to its highest turn-on voltage. The open-circuit voltage (V_{oc}) of DSSCs can be generally estimated by the difference between the quasi-Fermi level of electrons in TiO_2 and the electrochemical potential of the redox medium HTM/HTM$^+$ [42]. These values should be very close for devices based on T4MPCA, T2MPCA and spiro-OMeTAD, since they exhibit similar potentials [17]. Nevertheless, device using T4MPCA exhibits a V_{oc} of 0.74 V, 50 mV lower than the reference cell. The device using T2MPCA exhibits a V_{oc} of 0.73 V, 60 mV lower than the reference cell. The decrease of V_{oc} is associated with the decrease of *FF* for these cells compared to spiro-OMeTAD. Indeed, the *FF* is limited to 34% and 30% respectively for T4MPCA and T2MPCA although this value reaches 62% with the reference cell. Several factors can explain this trend. First, a poor TiO_2 pore filling by T4MPCA and T2MPCA could be responsible of a poor TiO_2/dye/HTM interface area and interface quality. According to the literature, an optimized concentration around 170–200 mg ml^{-1} [43] is required to obtain a suitable filling of the HTM inside the mesoporous TiO_2. This parameter is thus a key parameter to optimize the performance of solid-state DSSC [44]. We observed that the solubility of T4MPCA and T2MPCA in chlorobenzene at room temperature is largely lower than 200 mg ml^{-1}. Thus, heating the HTMs solutions at 150 °C and 180 °C respectively for T4MPCA and T2MPCA prior to electrode infiltration were required to completely solubilize the molecular glasses. It is therefore reasonable to suggest that the low solubility of T4MPCA and T2MPCA can induce a poor filling of the sensitized TiO_2 electrode, leading to a poor quality of the TiO_2/dye/HTM interface.

Moreover, a lower shunt resistance can be estimated for the new compounds compared to spiro-OMeTAD, associated to the reduced *FF* observed for T4MPCA (Table 4). This could indicate that the experimental conditions used for the HTM infiltration are not optimized. In particular, a residual HTM top layer is usually crucial for proper device operation [11,44] as it improves the selectivity of the gold top electrode for hole collection, reducing the apparent shunts. This parameter remains to be investigated for the T4MPCA

Table 4
Photovoltaic parameters.

Composition	J_{sc} [mA cm^{-2}]	V_{oc} [mV]	*FF* (%)	R_{sh} (Ω)	R_s (Ω)	Eff (%)
TiO_2/D102/Spiro/Au	8.15	790	62	10,112	110	3.94
TiO_2/D102/T4MPCA/Au	8.85	740	34	5260	266	2.23
TiO_2/D102/T2MPCA/Au	1.57	730	30	2113	2296	0.30

HTM. The T2MPCA compound is associated with a very poor photovoltaic effect, although a reasonable open-circuit voltage, similar to that of T4MPCA, is evidenced. Considering the quite similar electronic properties of T2MPCA and T4MPCA (energetic levels), the very low photocurrent (1.57 mA cm^{-2}) and high series resistance (>2 kOhms) observed for the device using the former seem to indicate that a very poor pore filling and interface quality, or poor charge transport properties occur. The lower solubility of T2MPCA compare to T4MPCA can explain this drop in performance; however, the electronic properties of the material can also be responsible of this observation, through low charge transport properties. Indeed, T2MPCA has the highest turn-on voltage indicating that the transport in this material is lower compared to T4MPCA and spiro-OMeTAD.

The incident photon-to-electron conversion efficiencies (IPCE) as a function of wavelength for the two solid-state DSSC (with T4MPCA and spiro-OMeTAD) are studied (Fig. 6c). Both devices exhibit comparable photocurrent responses in the range 320–650 nm. In particular, the contribution of the D102 dye to current generation is found to be very similar. No specific contribution of the HTM can be observed in the spectra.

T4MPCA device exhibits a PCE of 2.23% under standard solar emission. To the best of our knowledge, this value is one of the highest reported to date for single star-shaped p-type semiconductor materials [45]. Even if the efficiency is still lower than that of the standard HTM, significant improvements are expected by increasing the solubility of the molecule at room temperature to favor pore filling leading to larger *FF* and V_{oc} parameters.

Transient photovoltage decay measurements were performed to better interpret the photovoltaic performance of the devices. The recombination kinetics are estimated under open-circuit condition for solar cells based on spiro-OMeTAD and T4MPCA respectively. The corresponding decay times are plotted in Fig. 7. Recombination is found to be slightly slower at low light intensities for device based on compound T4MPCA compared to spiro-OMeTAD. Under high illumination intensities (up to 80 mW cm^{-2}), recombination is found to be faster for device based on compound T4MPCA compared to spiro-OMeTAD. A faster charge recombination for T4MPCA is consistent with the reduced open-circuit voltage observed in the *J*(*V*) characteristics under full sun for this device compared to spiro-OMeTAD. Moreover, the different slopes evidenced for both devices indicate that slightly different recombination mechanisms are occurring which could be due to change in the local configuration of the molecular glass in relation with D102. Further investigations are necessary to better understand these different recombination mechanisms.

To summarize, our analysis show interesting potentialities for the new star-shaped carbazole compounds developed in this work, especially for the T4MPCA molecular glass. The high photocurrent observed for this device is a consequence of suitable electronic properties. In particular, a suitable energetic configuration with regard to the organic D102 dye ensure an efficient regeneration mechanisms, leading to an impressive photocurrent density (8.85 mA cm^{-2}) if we consider the very poor fill factor (only 34%) that are evidenced in these non-optimized devices. Considering this current level, charge transport properties are likely to reach very descent values. We emphasize that in this context, the HTM

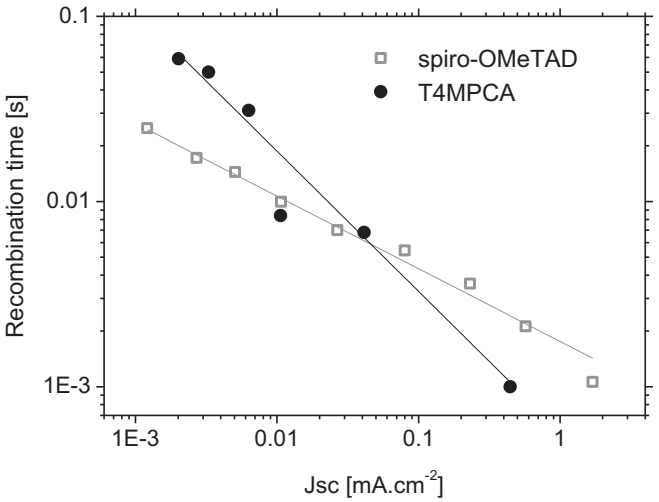

Fig. 7. Transient photovoltage and photocurrent characteristics of devices with T4MPCA (black circle) and spiro-OMeTAD (gray square).

charge mobility hence device *FF*, would also strongly benefit from doping strategies, keeping in mind that the highest efficiency to date of an organic dye-sensitized solid-state DSSC was achieved using a cobalt dopant [13]. Moreover, it is worth noting that optimized D102-sensitized solid state DSSCs usually deliver up to 9.3 mA cm^{-2} at best [28]. In this context, our T4MPCA device can be considered as a highly promising system. A careful optimization of the HTM deposition conditions, in order to ensure a high filling fraction and improved HTM overlayer, can reasonably lead to fill factors of at least 50%, leading to power conversion efficiencies in the order of 4%, indicating that this new HTM can efficiently compete with the existing reference.

4. Conclusion

Two star-shaped carbazole based molecular glasses were synthesized and their thermal, optical, photophysical, electrochemical properties were studied. These new HTM showed high glass transition temperatures at 164 °C and 175 °C respectively for T4MPCA and T2MPCA, as measured by differential scanning calorimetry. T4MPCA and T2MPCA exhibited high thermal stability with 5% weight loss temperatures of 490 °C and 480 °C, respectively. The star-shaped molecules showed absorption in the range of 225–450 nm and an estimated band gap of 2.75 eV. The tri(9-(methoxyphenyl)carbazol-3-yl)amines were found to be electrochemically stable; their cyclic voltammograms showed reversible oxidation behavior. The solid state ionization potential IPs of the star-shaped carbazole trimers were found to be 4.98 and 4.96 eV and well adapted to an efficient regeneration of the photo-oxidized dye. A typical solid state dye sensitizer solar cell was realized with T4MPCA and T2MPCA as hole transporting materials. Due to its higher solubility in chlorobenzene, T4MPCA is more filled in the porous oxide which improve its PV performances. Without device optimization, a power conversion efficiency of 2.23% was achieved with this new hole transporting material (T4MPCA) with a J_{sc} of 8.85 mA cm^{-2}, which is found to be higher than that of the reference device based on spiro-OMeTAD. These efficiencies are shown to be one of the highest known for star-shaped, triphenylamino type, molecules.

Acknowledgments

The support of this research from joint French-Lithuanian research program PHC GILIBERT 2013(Project N° 28415NC) is

gratefully acknowledged. This research was also funded by the European Social Fund under the Global Grant measure and Region Centre.

References

[1] M. Law, L.E. Greene, J.C. Johnson, R. Saykally, P. Yang, Nat. Mater. 4 (2005) 455–459.
[2] H.J. Snaith, M. Grätzel, Adv. Mater. 19 (2007) 3643–3647.
[3] B. O'Regan, M. Graetzel, Nature 353 (1991) 737–740.
[4] B.E. Hardin, H.J. Snaith, M.D. McGehee, Nat. Photon. 6 (2012) 162–169.
[5] M.K. Nazeeruddin, F. De Angelis, S. Fantacci, A. Selloni, G. Viscardi, P. Liska, S. Ito, B. Takeru, M. Graetzel, J. Am. Chem. Soc. 127 (2005) 16835–16847.
[6] C.-Y. Chen, M. Wang, J.-Y. Li, N. Pootrakulchote, L. Alibabaei, C.-H. Ngoc-le, J.-D. Decoppet, J.-H. Tsai, C. Graetzel, C.-G. Wu, S.M. Zakeeruddin, M. Graetzel, ACS Nano 3 (2009) 3103–3109.
[7] A. Yella, H.-W. Lee, H.N. Tsao, C. Yi, A.K. Chandiran, M.K. Nazeeruddin, E.W.-G. Diau, C.-Y. Yeh, S.M. Zakeeruddin, M. Graetzel, Science 334 (2011) 629–634.
[8] J.M. Kroon, N.J. Bakker, H.J.P. Smit, P. Liska, K.R. Thampi, P. Wang, S.M. Zakeeruddin, M. Grätzel, A. Hinsch, S. Hore, U. Würfel, R. Sastrawan, J.R. Durrant, E. Palomares, H. Pettersson, T. Gruszecki, J. Walter, K. Skupien, G.E. Tulloch, Prog. Photovolt. Res. Appl. 15 (2007) 1–18.
[9] A. Abrusci, R.S. Santosh Kumar, M. Al-Hashimi, M. Heeney, A. Petrozza, H.J. Snaith, Adv. Funct. Mater. 21 (2011) 2571–2579.
[10] P. Docampo, A. Hey, S. Guldin, R. Gunning, U. Steiner, H.J. Snaith, Adv. Funct. Mater. 22 (2012) 5010–5019.
[11] H.J. Snaith, R. Humphry-Baker, P. Chen, I. Cesar, S.M. Zakeeruddin, M. Graetzel, Nanotechnology 19 (2008) 424003–424015.
[12] L. Schmidt-Mende, U. Bach, R. Humphry-Baker, T. Horiuchi, H. Miura, S. Ito, S. Uchida, M. Grätzel, Adv. Mater. 17 (2005) 813–815.
[13] J. Burschka, A. Dualeh, F. Kessler, E. Baranoff, N.-L. Cevey-Ha, C. Yi, M.K. Nazeeruddin, M. Graetzel, J. Am. Chem. Soc. 133 (2011) 18042–18045.
[14] J. Burschka, N. Pellet, S.-J. Moon, R. Humphry-Baker, P. Gao, M.K. Nazeeruddin, M. Graetzel, Nature 499 (2013) 316–319.
[15] G. Puckyte, B. Schmaltz, A. Tomkeviciene, M. Degbia, J.V. Grazulevicius, H. Melhem, J. Bouclé, F. Tran-Van, J. Power Sources 233 (2013) 86–92.
[16] A. Tomkeviciene, G. Puckyte, J.V. Grazulevicius, M. Degbia, F. Tran-Van, B. Schmaltz, V. Jankauskas, J. Bouclé, Synth. Met. 162 (2012) 1997–2004.
[17] T. Leijtens, I.K. Ding, T. Giovenzana, J.T. Bloking, M.D. McGehee, A. Sellinger, ACS Nano 6 (2012) 1455–1462.
[18] K. Masatane, Nippon Kagaku Zasshi 88 (1967) 463–468.
[19] D. Bogdal, Patent 887188, 2001.
[20] H. Shigeru, T. Masato, M. Masaki, Patent, JPH 0841327, 1996
[21] M. Lux, P. Strohriegl, H. Höcker, Die Makromol. Chem. 188 (1987) 811–820.
[22] S.H. Tucker, J. Chem. Soc. 129 (1926) 546–553.
[23] E. Miyamoto, Y. Yamaguchi, M. Yokoyama, Denshi Shashin Gakkaishi (Electrophotography) 28 (1989) 364–370.
[24] T. Malinauskas, M. Daskeviciene, K. Kazlauskas, H.-C. Su, J.V. Grazulevicius, S. Jursenas, C.-C. Wu, V. Getautis, Tetrahedron 67 (2011) 1852–1861.
[25] L. Kavan, M. Graetzel, Electrochim. Acta 40 (1995) 643–652.
[26] H.J. Snaith, L. Schmidt-Mende, M. Graetzel, M. Chiesa, Phys. Rev. B 74 (2006) 045306.
[27] L. Vesce, R. Riccitelli, G. Soscia, T.M. Brown, A. Di Carlo, A. Reale, J. Non-Cryst. Sol. 356 (2010) 1958–1961.
[28] H. Melhem, P. Simon, L. Beouch, F. Goubard, M. Boucharef, C. Di Bin, Y. Leconte, B. Ratier, N. Herlin-Boime, J. Bouclé, Adv. Energy Mater. 1 (2011) 908–916.
[29] J.M. Kroon, M.M. Wienk, W.J.H. Verhees, J.C. Hummelen, Thin Solid Films 403–404 (2002) 223–228.
[30] U. Bach, D. Lupo, P. Comte, J.E. Moser, F. Weissortel, J. Salbeck, H. Spreitzer, M. Gratzel, Nature 395 (1998) 583–585.
[31] J.F. Ambrose, L.L. Carpenter, R.F. Nelson, J. Electrochem. Soc. 122 (1975) 876–894.
[32] Y. Qiao, Z. Wei, C. Risko, H. Li, J.-L. Bredas, W. Xu, D. Zhu, J. Mater. Chem. 22 (2012) 1313–1325.
[33] X. Zhan, C. Risko, F. Amy, C. Chan, W. Zhao, S. Barlow, A. Kahn, J.L. Brédas, S.R. Marder, J. Am. Chem. Soc. 127 (2005) 9021–9029.
[34] B.R. Kaafarani, A.a.O. El-Ballouli, R. Trattnig, A. Fonari, S. Sax, B. Wex, C. Risko, R.S. Khnayzer, S. Barlow, D. Patra, T.V. Timofeeva, E.J.W. List, J.-L. Bredas, S.R. Marder, J. Mater. Chem. C 1 (2011) 1638–1650.
[35] A. Tomkeviciene, J.V. Grazulevicius, K. Kazlauskas, A. Gruodis, S. Jursenas, T.-H. Ke, C.-C. Wu, J. Phys. Chem. C 115 (2011) 4887–4897.
[36] S. Grigalevicius, G. Blazys, J. Ostrauskaite, J.V. Grazulevicius, V. Gaidelis, V. Jankauskas, J. Photochem. Photobiol. A Chem. 154 (2003) 161–167.
[37] J. Krueger, R. Plass, M. Graetzel, H.-J. Matthieu, Appl. Phys. Lett. 81 (2002) 367–369.
[38] S.A. Haque, E. Palomares, B.M. Cho, A.N.M. Green, N. Hirata, D.R. Klug, J.R. Durrant, J. Am. Chem. Soc. 127 (2005) 3456–3462.
[39] S.A. Haque, T. Park, C. Xu, S. Koops, N. Schulte, R.J. Potter, A.B. Holmes, J.R. Durrant, Adv. Funct. Mater. 14 (2004) 435–440.
[40] R. Zhu, C.-Y. Jiang, B. Liu, S. Ramakrishna, Adv. Mater. 21 (2009) 994–1000.
[41] K. Hara, T. Sato, R. Katoh, A. Furube, Y. Ohga, A. Shinpo, S. Suga, K. Sayama, H. Sugihara, H. Arakawa, J. Phys. Chem. B 107 (2002) 597–606.
[42] X. Jiang, K.M. Karlsson, E. Gabrielsson, E.M.J. Johansson, M. Quintana, M. Karlsson, L. Sun, G. Boschloo, A. Hagfeldt, Adv. Funct. Mater. 21 (2011) 2944–2952.
[43] I.K. Ding, J. Melas-Kyriazi, N.-L. Cevey-Ha, K.G. Chittibabu, S.M. Zakeeruddin, M. Graetzel, M.D. McGehee, Org. Electron. 11 (2010) 1217–1222.
[44] I.K. Ding, N. Tétreault, J. Brillet, B.E. Hardin, E.H. Smith, S.J. Rosenthal, F. Sauvage, M. Grätzel, M.D. McGehee, Adv. Funct. Mater. 19 (2009) 2431–2436.
[45] N. Metri, X. Sallenave, C. Plesse, L. Beouch, P.-H. Aubert, F. Goubard, C. Chevrot, G. Sini, J. Phys. Chem. C 116 (2012) 3765–3772.